ISBN: 978-3-95450-231-8 ISSN: 2673-5490 doi: 10.18429/JACoW-IPAC2023-WEPM043

STATUS OF MAGNET SYSTEMS FOR KOREA 4GSR*

D. E. Kim†, Y. G. Jung, I-W Chun, H. S. Suh, H. G. Lee, and J. Lee
Pohang Accelerator Laboratory, POSTECH, Pohang, KyungBuk, Republic of Korea

Abstract

A 4th generation storage ring based light source is being developed in Korea since 2021. It features < 100 pm rad emittance, about 800 m circumference, 4 GeV e-beam energy, full energy booster injection, and more than 40 beamlines which includes more than 24 insertion device (ID) beamlines. This machine requires about 1300 magnets including dipole, longitudinal gradient dipole, transverse gradient dipole, sextupoles, and correctors. In this report, the current status and prototyping status of some key magnets are presented. Particularly, impact of the end chamfering of the quadrupole magnet on the integrated multipoles are analyzed and optimum and (hopefully universal) chamfering profile is suggested.

INTRODUCTION

Third generation storage ring based light sources have been used as a bright light source for many years. Recently multi-bend achromat (MBA) lattice presents a further decrease in the electron beam emittances and becoming a new standard for next generation light source. Korea is trying to build a 4th generation light source (Korea-4GSR) based on modified hybrid multi-bend achromat lattice (MHMBA). The Korea lattice design for Korea-4GSR was described in [1], and recently updated to have high beta long straight section to increase dynamic aperture, and life time [2]. The storage ring lattice requires about 1044 magnets, while booster requires more than 306 magnets. LGBM magnet is described in the 4, and we focus on the quadrupole ans sextupole design in this report.

We can describe the 2-dimensional accelerator magnetic field using simple complex potential [3,4]. For pure, normal magnet where the magnetic field is normal to the midplane, we can see a_n is a normal component of the multipole content of the magnet in Eq. (1). In terms of a polar coordinate $z = x + iy = re^{i\theta}$, we can express the $B_y(\theta)$ along the radius r as

$$B_y(r,\theta) = \sum_{n=1}^{\infty} \frac{-na_n}{r_0}\left(\frac{r}{r_0}\right)^{n-1} \cos((n-1)\theta) \qquad (1)$$

Please note that in this indexing scheme, $n = 1$ is dipole, $n = 2$ is quadrupole, $n = 3$ is a sextupole components. In analyzing a magnet, we calculate the B_y along a circle at a slice (usually 1 mm thick) and decompose it according to Eq. (1) to analyze the longitudinal dependence of a multipole content.

QUADRUPOLES, QUAD-BENDS MAGNETS

There are four mechanical kinds of Quad-Bends, while 4 kinds of mechanical quadrupole types are required. Among the four kinds of quad-bends, one is positive bending magnet, and remaining three types are reverse bends to optimized the beam emittances. The quad-bend design is reported in ref [5]. In this section, we focus on the quadrupole series with aperture radius of 15 mm having 4 kinds of magnetic length 145 mm, 200 mm, 250 mm, 385 mm, respectively. The maximum field gradient is 60 T/m and good field radius is 10 mm with maximum allowed multipole strength at good field radius should be less than 1.0×10^{-3}. Also minimum pole to pole distance should be greater than ±5.0 mm and photon slots for photon extraction from the bending, and the insertion device should be provided. The pole and coil geometry needed several iteration to avoid any mechanical interference with vacuum chamber.

2D optimization is carried out using conformal mapping [3,4]. 2D dipole geometry is seup first with pole width meeting the pole to pole distance requirements in real geometry. This pole to pole distance requirements actually translates to pole width in the dipole geometry which is important parameter for overall field quality. Pole shims are introduced in dipole geometry and the geometry is translated to real quadrupole geometry using the conformal map given by

$$w = u + iv = \frac{(x+iy)^2}{2r_c} \qquad (2)$$

The field quality in real quadrupole geometry is calculated while changing the shim geometry in the dipole plane. With this procedure, the impact of the shims on the multipole can be easily calculated. After 2D optimization, 3D calculations are done to assess the longitudinal dependence of the fundamental and higher harmonic content as shown in Fig. 1.

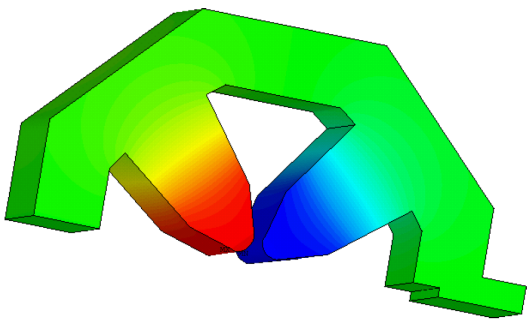

Figure 1: 3D FEM analysis of the quadrupole.

* Work supported by MSIT of Korea
† dekim@postech.ac.kr

ISBN: 978-3-95450-231-8 ISSN: 2673-5490 doi: 10.18429/JACoW-IPAC2023-WEPM043

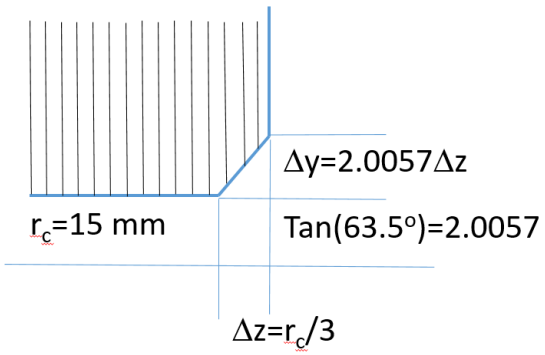

Figure 2: Pole end chamfering of the quadrupole magnet. Chamfering depth Δz, and chamfering angle is the control parameter.

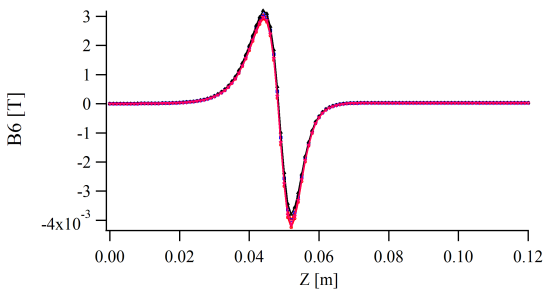

Figure 3: The typical longitudinal profile of the 1st allowed multipole content b6 at r=10 mm with different chamfering . The next lowest allowed multipole is B10 and B10 is small and not so sensitive to the chamfering.

To optimize in 3D geometry, pole ends are cut in a plane like chamfering. The depth, and angle of the chamfering cut it the optimization parameter. The chamfer geometry is shown in Fig. 2.

Table 1: Major Parameters of Quadrupole Magnet

Parameter	Values		
Magnet Type	Q11/Q52	Q12/31/32	Q51
Required Num.	56/56	56/56/56	56
Max B' [T/m]	60.0	60.0	60.0
Multipole	< 1.0E-3	1.0E-3	1.0E-3
Rc [mm]	15.0	15.0	15.0
L_{eff} [m]	200.0	145.0	384.0
Trim winding	No	No	No
Amp. Turns [kA]	5.71	5.71	5.71
Conductor	6.5x6.5x4ϕ	<-	<-
Num. Turns	56	56	56
Imax [A]	102.0	102.0	102.0
Js [A/mm^2]	3.54	3.54	3.54
V	9.31	7.70	14.7
# Cool. Cir.	2	2	4
ΔT [K]	6.5	4.9	4.7
Δp [bar]	6.0	6.0	6.0

The typical longitudinal profile of the 1st allowed multipole content B6 at r=10 mm with different chamfering is shown in Fig. 3. It can be seen that the edge contribution of the longitudinal distribution of B6 does not integrate to zero. If the integration of the edge contribution of B6 is not zero, we may need to keep some B6 in the body region to achieve integrated B6 zero. Several chamfering depth, and cut angle is tried and the integrated B6 is calculated from the far side of the magnet to the center of the magnet to remove the effect of any residual B6 in the body region of the magnet. The results is shown in Fig. 4. At this chamfering depth, and chamfering angle, the edge contribution is canceled at the edge. Since the edge contribution is canceled at the edge, we can use same chamfering for quadrupoles with different magnetic length. If edge contribution is not compensated at the edge, the integrated B6 depends on the magnetic length and the chamfering geometry should be different for different length quadrupoles. Also, since the magnet is not saturate, the problem is almost linear, and the end cut can be scaled for other aperture radius. We tested it for 20 mm aperture quadrupole magnet, and the edge compensation was still very good. Major parameter of the quadrupole magnets are shown in Table 1 for three types of quadrupoles with magnetic length of 145 mm, 200 mm, 384 mm.

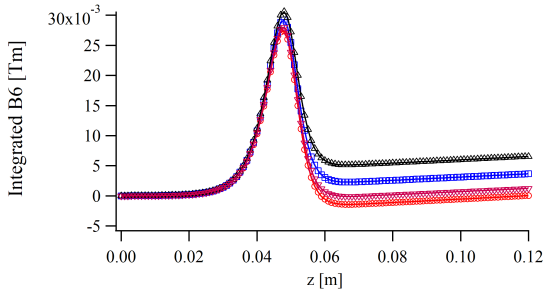

Figure 4: The integral of the B6 from the far side of the magnet. At chamfer depth Δz =5 mm, 63.5 degree cut gave the best results.

SEXTUPOLE MAGNET

Previously, there was only 1 kind of sextupole with effective length of 250 mm. The lattice is updated to have two longer high beta straight section to increase the dynamic aperture, and injection efficiency. Also 2 octupole magnets are newly added to the lattice which required shortening the longitudinal length of other magnets. Due to this, the sextupole length was decreased to 180 mm, and 200 mm. The maximum field strength in terms of the 2nd derivative is 2084 T/m^2. Also there was a requirement of minimum pole to pole distance of $\pm$6.5 mm which was necessary from the vacuum chamber design. Another issue was the extraction of photon beam when the EPUs are operated in pure vertical mode. The vertical power distribution was about 1.1 mrad including the undulator orbit interlock allowance. The photon fan is described in Fig. 5. The three positions of the photon fan represents three different position of the

ISBN: 978-3-95450-231-8 ISSN: 2673-5490 doi: 10.18429/JACoW-IPAC2023-WEPM043

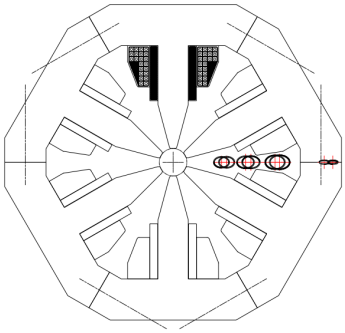

Figure 5: Photon fan of the EPU in vertical mode. The photon fans show three difrerent sextupole position. The photon fan shown in the yoke represents photon fan from the bending source.

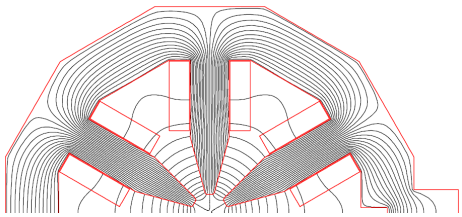

Figure 6: 2D flux distribution and yoke geometry with flat pole tip.

sextupole magnet. To meet this requirements, the aperture radius of the sextupole magnet is increased to 20 mm giving maximum pole tip field of 0.42 T which is quite acceptable. However, the sextupoles are expected to operate as horizontal corrector, vertical corrector, skew quadrupole magnet. The corrector strength is 600μrad kick at 4 GeV which requires rather big auxiliary coil size as shown in Fig. 5 and when all trim magnets are excited at their rated value, the pole tip starts to saturate. Since the trim winding correctors in the sextupole magnet is only used for slow correction, the sextupole magnet will be manufactured using solid core.

Minimum pole to pole distane of ±6.5 mm is effectively limiting the pole width which deteriorated the multipole content. With optimized pole tip, the multipole at good field radius of $r_0 = 10$ mm is about 2×10^{-4}. The small multipole contents resulted from the increased aperture radius (r_c = 20 mm) and smaller good field region ($r_0 = 10$ mm). 2D optimization is done adding usual tangential shims from the ideal pole profile. But since the effective pole width is so small, the tangential shim should start at the pole center effectively making flat pole tip. the 2D field profile is shown in the Fig. 6.

The interference of the main sextupole components with h-corrector/v-corrector/skew-quadrupole are evaluated. While changing the sextupole excitation from 0 to nominal value, the normalized strength of the H/V corrector, and skew quadrupole strength is calculated to estimate the impact of the saturation. The results is shown in Fig. 7 showing maximum decrease of skew quadrupole component by 5 %.

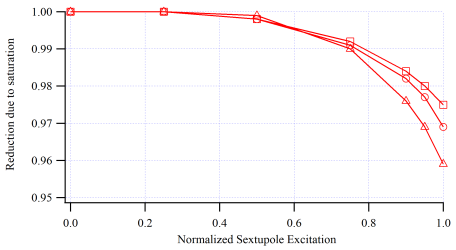

Figure 7: The effect of sextupole excitation on the normalized strength of the auxiliary components. Square is H-corrector, Circle is V-corrector, triangle is skew quadrupole components.

The reduction in H-corrector, V-corrector is about 2.5 %, 3.0 % which is small enough and acceptable.

After 2D optimization, 3D calculations are done to assess the longitudinal dependence of the fundamental and higher harmonic content (particularly the fist two allowed harmonic of B9, B15). The results are shown in Fig. 8. The multipole content is order of $\sim 2.0 \times 10^{-4}$ which is well within the requirement of 1.0×10^{-3}.

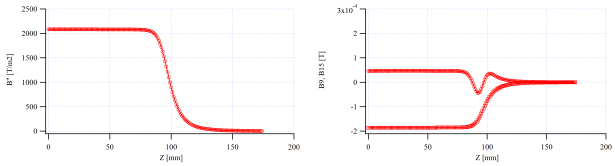

Figure 8: B" distribution (left), B9, B15 at r=10 mm along the magnet(right).

SUMMARY

Korea 4th generation synchrotron radiation source project going on targetting installation at 2027. Storage ring requires more than 1044 magnets in addition to 306+ booster magnets. In this report, the 2D, design efforts for the SR quadrupoles, and sextupoles are described. Particularly, 3D optimization is done to cancel out the edge contribution of B6 multipole at the edge. So that the same chamfering can be used for different length of the quadrupoles. Also, since the magnet is not saturated, the design can be scaled to other aperture. Sextupole pole tip optimiation converged to a flat pole face. 3D simulation showed that the multipoles were well within the beam dynamics requirements. Prototyping contracts are expected soon.

ACKNOWLEDGEMENTS

This research was supported in part by the korean Government MSIT (Multipurpose Synchrotron Radiation Construction Project) and by the Basic Science Research Program through the National Research Foundation of Korea (NRF-2019R1A2C1004862).

ISBN: 978-3-95450-231-8 ISSN: 2673-5490 doi: 10.18429/JACoW-IPAC2023-WEPM043

REFERENCES

[1] G. S. Jang, S. Shin, M. Yoon, J. Ko, Young Dae Yoon, J. Lee, B-H. Oh, "Low emittance lattice design for Korea-4GSR", *Nucl. Instrum. Methods Phys. Res., Sect. A*, vol. 1034, p. 166779, 2022. doi:10.1016/j.nima.2022.166779

[2] G. Jang, J. Kim, D. E. Kim, J. Lee, J. Seok, and T. Ha, "Korea-4GSR Lattice Update", presented at the IPAC'23, Venice, Italy, May 2023, paper WEPL058, this conference.

[3] K. Halbach, "First order perturbation effects in iron-dominated two-dimensional symmetrical multipoles", *Nuclear Instruments and Methods*, vol. 74, pp. 147–164, 1969. doi:10.1016/0029-554X(69)90502-3

[4] D. E. Kim *et al.*, "Magnet Systems for Korea 4GSR Light Source", in *Proc. IPAC'22*, Bangkok, Thailand, Jun. 2022, pp. 2781–2783. doi:10.18429/JACoW-IPAC2022-THPOTK007

[5] H. Suh, Y. Jung, S.-H. Jeong, H.-G. Lee, D. E. Kim, and I. Chun, "Dipole quadrupole magnet design for Korea-4GSR", presented at the IPAC'23, Venice, Italy, May 2023, paper WEPM044, this conference.